



Seismic velocity structure across the 2013 Craig, Alaska rupture from aftershock tomography: Implications for seismogenic conditions

Maureen A.L. Walton^{a,*}, Emily C. Roland^b, Jacob I. Walter^{a,2}, Sean P.S. Gulick^a, Peter J. Dotray^{a,3}

^a The University of Texas Institute for Geophysics, J. J. Pickle Research Campus, 10100 Burnet Rd. (R2200), Austin, TX 78758, United States

^b The University of Washington, School of Oceanography, 1503 NE Boat St., Seattle, WA 98105, United States

ARTICLE INFO

Article history:

Received 18 April 2018

Received in revised form 1 November 2018

Accepted 9 November 2018

Available online xxxx

Editor: M. Ishii

Keywords:

seismicity
tomography
supershear
earthquake
aftershock
strike-slip

ABSTRACT

The 2013 Craig, Alaska M_W 7.5 earthquake ruptured along ~ 150 km of the Queen Charlotte Fault (QCF), a right-lateral strike-slip plate boundary fault separating the Pacific and North American plates. Regional shear wave analyses suggest that the Craig earthquake rupture propagated in the northward direction faster than the S-wave (supershear). Theoretical studies suggest that a bimaterial interface, such as that along the QCF, which separates oceanic and continental crust with differing elastic properties, can promote supershear rupture propagation. We deployed short-period ocean-bottom seismometers (OBS) as a part of a rapid-response effort less than four months after the Craig earthquake mainshock. During a 21-day period, 1,133 aftershocks were recorded by 8 OBS instruments. Aftershock spatial distribution indicates that the base of the seismogenic zone along the QCF approaches ~ 25 km depth, consistent with a thermally-controlled fault rheology expected for igneous rocks at oceanic transform faults. The spatial distribution also provides supporting evidence for a previously hypothesized active strand of the QCF system within the Pacific Plate. Tomographic traveltime inversion for velocity structure indicates a low-velocity (V_P and V_S) zone on the Pacific side of the plate boundary at 5–20 km depths, where Neogene Pacific crust and upper mantle seismic velocities average ~ 3 –11% slower than the North American side, where the Paleozoic North American crust is seismically faster. Our results suggest that elastic properties along the studied portion of the QCF are different than those of a simple oceanic–continental plate boundary fault. In our study region, velocity structure across the QCF, while bimaterial, does not support faster material on the west side of the fault, which has been proposed as one possible explanation for northward supershear propagation during the Craig earthquake. Instead, we image low-velocity material on the west side of the fault. Explanations could include that part of the rupture was subshear, or that fault damage zone properties or fault smoothness are more important controls on supershear rupture than a bimaterial contrast.

Published by Elsevier B.V.

1. Introduction

The Queen Charlotte Fault (QCF) is a NW-striking, right-lateral strike-slip fault that forms the plate boundary between the Pacific and North American tectonic plates offshore of western Canada stretching northward to southeastern Alaska (Fig. 1). The north-

ern end of the QCF is marked by an offshore–onshore transition to the Fairweather Fault, with the offshore length of the Fairweather–Queen Charlotte strike-slip system totaling ~ 900 km (Fig. 1). Historical seismicity indicates that the QCF is a seismically active fault system capable of rupturing in magnitude > 7 events and thus poses a hazard to communities in western Canada and southeastern Alaska. The offshore QCF has ruptured in several large earthquakes in the past century, including the M_W 8.1 Queen Charlotte earthquake in 1949, which ruptured ~ 265 km of the southern QCF (Bostwick, 1984); the M_W 7.6 Sitka event in 1972, which ruptured a segment north of the 1949 event (Schell and Ruff, 1989; Doser and Rodriguez, 2011); and recently, a M_W 7.8 event along the southernmost QCF near Haida Gwaii, British Columbia in 2012 (e.g., Lay et al., 2013), followed by a M_W 7.5 event overlapping

* Corresponding author.

E-mail address: mwalton@usgs.gov (M.A.L. Walton).

¹ Now at: Pacific Coastal and Marine Science Center, U.S. Geological Survey, 2885 Mission St., Santa Cruz, CA 95060, United States.

² Now at: Oklahoma Geological Survey, University of Oklahoma, 100 E Boyd St., Norman, OK 73019, United States.

³ Now at: Hawaiian Volcano Observatory, U.S. Geological Survey, Reggie Okamura Building, Crater Rim Road, Hawaii National Park, HI 96718, United States.

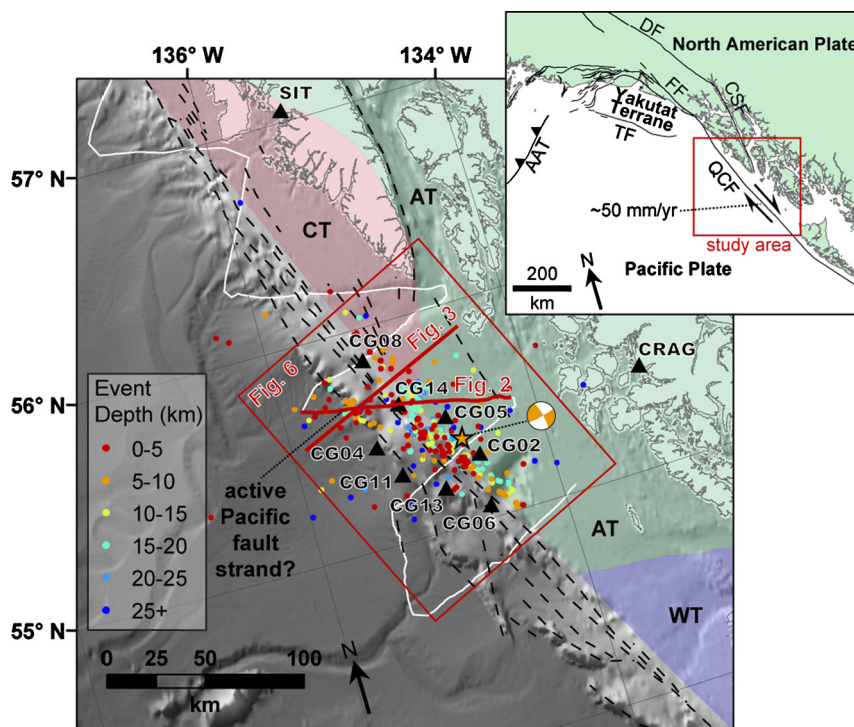


Fig. 1. Map showing Craig earthquake area. Background shows grayscale bathymetry from Smith and Sandwell (1997) and the United Nations Convention on the Law of the Sea (UNCLOS). North America terranes are shown as transparent overlays (Colpron and Nelson, 2011): AT – Alexander Terrane, CT – Chugach Terrane, WT – Wrangellia Terrane. Aftershock epicenters used in this study are colored by depth (warm = shallow, cool = deep). An orange star and focal mechanism (U.S. Geological Survey (USGS), earthquake.usgs.gov) highlight the M_w 7.5 Craig mainshock epicenter. Labeled black triangles are the passive-source stations used in this study, including land stations and the 8 rapid-response OBS instruments (labeled CG*). Dashed black lines are fault traces mapped from legacy data by Walton et al. (2015), including a potentially active fault within the Pacific Plate as indicated by aftershocks identified in this study. White lines indicate tracklines from the USGS seismic reflection survey L378EG, and red lines show the locations of the profile in Fig. 2 and the cross-section in Fig. 3. A red box outlines the location of Fig. 6. Inset shows the regional setting and major tectonic features: QCF – Queen Charlotte Fault, FF – Fairweather Fault, DF – Denali Fault, CSF – Chatham Strait Fault, TF – Transition Fault, and AAT – Alaska-Aleutian Trench. (For interpretation of the colors in the figure(s), the reader is referred to the web version of this article.)

the northernmost 1949 rupture near Craig, Alaska in 2013 (e.g., Yue et al., 2013). Although the QCF sustains events of comparable moment release to the San Andreas Fault (e.g., Fletcher and Freymueller, 2003), much less is known about the QCF margin in large part due to its remote offshore location.

The 5 January 2013 Craig earthquake was a M_w 7.5 right-lateral, strike-slip event that ruptured ~ 150 km of the mapped plate boundary (e.g., Aderhold and Abercrombie, 2015). Regional shear wave analysis and high-rate GPS were used to infer that the Craig rupture propagated northward at speeds of 5.5–6 km/s (Yue et al., 2013), assuming a seismogenic depth range of 0–10 km. A rupture propagation velocity of 5.5–6 km/s would exceed the S-wave velocity and approach the P-wave velocity along the fault between 0–10 km depths (Horn et al., 1984), creating a supershear rupture in the northward direction (Yue et al., 2013).

Supershear rupture has rarely been observed during real earthquakes (e.g., Dunham and Archuleta, 2004), and there are several hypotheses for the conditions under which supershear ruptures occur. Numerical models of unilateral supershear ruptures, in which fault rupture nucleates and then propagates in mostly one direction, suggest that supershear ruptures may occur along bimaterial interfaces. A bimaterial interface is a fault plane with a significant contrast in elastic properties on either side of the fault (Xia et al., 2005; Shi and Ben-Zion, 2006). Alternatively, Bouchon et al. (2010) compiled available global observations of supershear rupture, noting that documented supershear ruptures always occur along geometrically simple, smooth, linear faults with highly localized and narrow deformation zones. Supershear transients along geometrically smooth fault segments have also been successfully modeled in numerical simulations (Bruhat et al., 2016), potentially

supporting the hypothesis that smooth fault geometry is important for promoting sustained supershear rupture.

The setting of the Craig earthquake along an oceanic–continental strike-slip fault suggests that supershear rupture could occur along bimaterial interface (Yue et al., 2013). Along a bimaterial interface, supershear ruptures may propagate in the direction of motion of the seismically faster side of the fault (Xia et al., 2005). In the case of the Craig event, if one assumes that Pacific Plate oceanic crust is stiffer at seismogenic depths, supershear rupture propagation would be expected in the northward direction (Yue et al., 2013). Such an assumption of relative seismic velocities might be expected for a simple oceanic–continental boundary.

Our study utilizes aftershocks of the 2013 Craig earthquake to test the broad-scale structure and the degree to which the QCF zone may consist of a bimaterial interface, consistent with theoretical conditions for supershear rupture. Sparse reflection and refraction studies, largely conducted before 1990 (von Huene et al., 1979; Horn et al., 1984; Dehler and Clowes, 1988; Mackie et al., 1989; Spence and Asudeh, 1993; Rohr et al., 2000), and geologic mapping throughout southeast Alaska (Plafker et al., 1989) provide somewhat limited information on the crustal structure along the offshore QCF in our study area. We provide new constraints on seismogenic zone geometry and crustal seismic velocities in the vicinity of the Craig rupture, utilizing a dataset of aftershocks recorded from the 2013 Craig event on an array of 8 ocean-bottom seismometers (OBS; Fig. 1). We use these data to invert for a model of P- and S-wave seismic velocity structure across the QCF in the region of the Craig earthquake. Our results shed light on the physical conditions along the QCF that may influence earthquake ruptures.

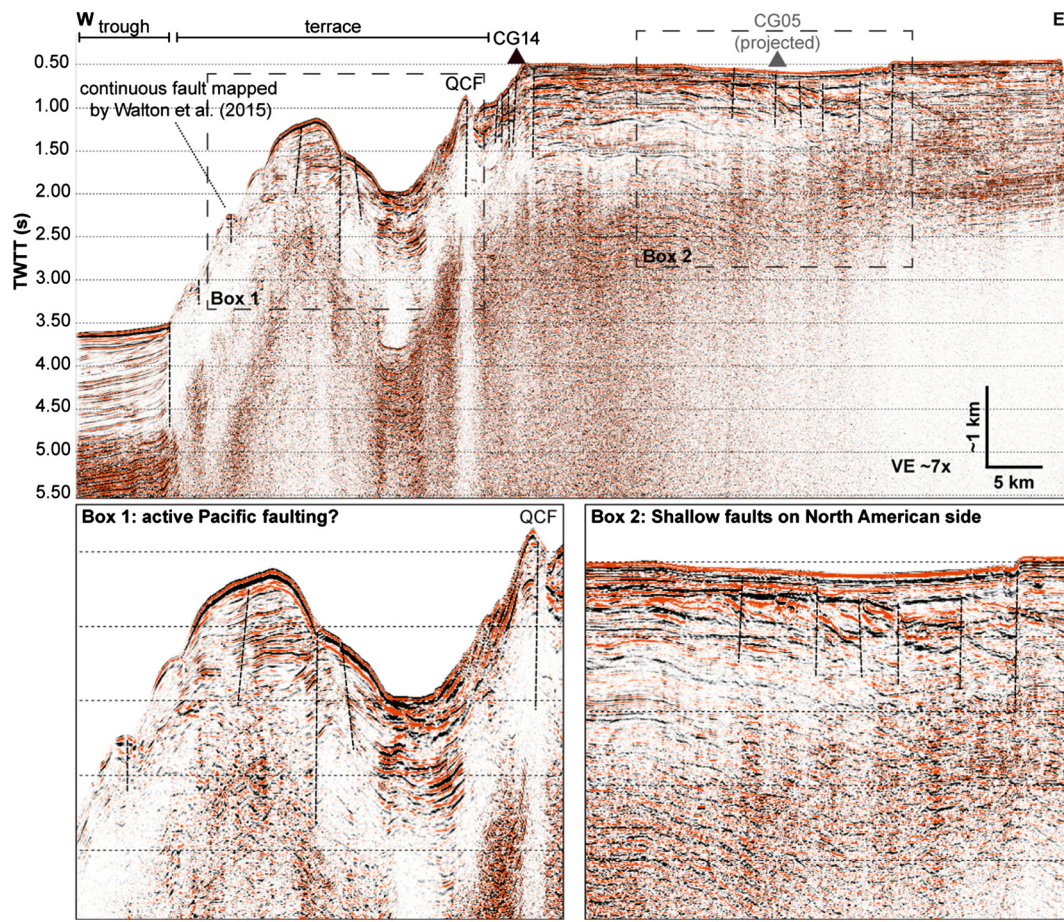


Fig. 2. Reprocessed USGS 2D seismic reflection profile L378EG.954. Interpreted faults are indicated by dashed lines in the subsurface, with the QCF and other potential fault strands dashed. The two nearest OBS instruments (black and gray triangles) are plotted for context. Box zooms highlight potentially active shallow crustal faults. Line location shown in Fig. 1. (For interpretation of the colors in the figure(s), the reader is referred to the web version of this article.)

2. Regional setting

The QCF is unusual in that it separates continental crust from oceanic crust; many strike-slip plate boundary fault systems go through the weaker (i.e., continental) side (e.g., San Andreas; ten Brink et al., 2018). At the plate boundary, the QCF system accommodates somewhere from ~ 44 mm/yr to over 50 mm/yr of right-lateral offset between the Pacific Plate and the North American Plate according to tectonic and geologic models (Fig. 1; Elliott et al., 2010; DeMets and Merkouriev, 2016; Brothers et al., 2017). To the north, where the QCF extends onshore at approximately $\sim 58.5^\circ\text{N}$, the Fairweather Fault accommodates ~ 50 mm/yr right-lateral offset between North American and the Yakutat Terrane, a thick oceanic crustal plateau, which is wedged in between and generally traveling with the Pacific Plate (Fig. 1; Christeson et al., 2010; Elliott et al., 2010; Gulick et al., 2013). The southern end of the QCF is located at a triple junction associated with the Explorer Plate. At its southern extent, the QCF meets the Revere–Dellwood Fault, another right-lateral strike-slip system (e.g., Rohr, 2015). Some form of transform motion has existed along the Queen Charlotte plate boundary since a major plate reorganization ca. 50 Ma (Haeussler et al., 2003). When the Yakutat Terrane began moving concurrently with the Pacific Plate ca. 20 Ma, the QCF assumed its current form as a right-lateral strike-slip fault (e.g., Hyndman and Hamilton, 1993).

The QCF is a near-vertical fault located within the Queen Charlotte Terrace, the deformed slope at the seaward limit of the North American shelf (e.g., Rohr et al., 2000; Fig. 2). The main trace of the QCF is visible in GLORIA sidescan sonar data (Bruns et al.,

1992), which constrain the fault maps we present here (Fig. 1), but several additional fault strands are also evident in seismic reflection data within and south of our study area (Tréhu et al., 2015; Walton et al., 2015; Fig. 1, Fig. 2). The dominantly strike-slip northern segment of the QCF, which includes the 2013 Craig earthquake rupture zone, extends between 53.2°N and the transition to the onshore Fairweather Fault. A slight clockwise shift in the vector of the Pacific Plate, which likely occurred sometime between ~ 12 and ~ 6 Ma (Dubrovine and Tarduno, 2008; DeMets and Merkouriev, 2016), led to increased convergence along the QCF, particularly in the south, potentially leading to splay faulting and Pacific Plate underthrusting as a way to accommodate convergent stress (e.g., Hyndman and Hamilton, 1993; Rohr et al., 2000; Tréhu et al., 2015; Walton et al., 2015). The 2012 M_W 7.8 Haida Gwaii thrust earthquake occurred in the southern region offshore of Haida Gwaii, and several recent studies (e.g., Lay et al., 2013) attribute this event to Pacific underthrusting.

The Pacific side of the QCF is geologically young, with age increasing northward from zero-age crust at the actively extending Explorer triple junction to ~ 20 Myr old crust near the Yakutat Terrane. There are thick sedimentary deposits overlying the Pacific crust due to the Baranof deep-sea fan system (Walton et al., 2014), and adjacent to the continental slope, a topographic “trough” along the central QCF has been associated with past convergence in this area (Walton et al., 2015; Fig. 2). Downwarping of the Pacific Plate due to underthrusting possibly led to increased accommodation space for sedimentary accumulation, introducing further load onto the plate and preserving Pacific Plate flexure (Walton et al., 2015). The thickest sedimentary deposits are therefore atop the Pacific

Plate nearest the QCF, within the Queen Charlotte Trough and the deformed Queen Charlotte Terrace slope sediments (Rohr et al., 2000; Tréhu et al., 2015; Fig. 2). Near the 2013 Craig event, the seismic velocities of the Pacific crust and sedimentary deposits are only constrained by a few local refraction profiles (von Huene et al., 1979), which show faster Pacific crustal velocities and support a thick sedimentary deposit within the Queen Charlotte Trough.

East of the QCF, the North American crust is composed of a complex series of late Paleozoic accreted terranes, namely the Alexander and Wrangellia terranes, with the Chugach Terrane located to the north of these (Plafker et al., 1989; Colpron and Nelson, 2011; Fig. 1). Basement outcrops exist nearest the QCF at Haida Gwaii, a group of islands located just to the south of the Craig event and on the North American side of the plate boundary; the islands are largely composed of exposed Wrangellia Terrane (Coney et al., 1980; Colpron and Nelson, 2011). The Alexander and Wrangellia terranes were contiguous by at least the mid-Pennsylvanian and accreted to North America during the Mesozoic (Gardner et al., 1988). These accreted terranes likely have faster seismic velocities than typical granitic continental crust. The Alexander and Wrangellia terranes, together often called the Insular Superterrane, contain low-grade metamorphic and Mesozoic basalts overlain by carbonate and chert (Coney et al., 1980; Plafker et al., 1989). Morozov et al. (1998) utilized rock-type velocity studies (e.g., Christensen and Mooney, 1995) to estimate compressional seismic wave velocities in the range of 5.7–6.0 km/s for the upper 5 km of Insular Superterrane crust, with higher velocity estimates at deeper crustal depths and where plutons were present. A refraction study south of where the Craig event occurred (Spence and Asudeh, 1993) found velocities of 6.5–7.2 km/s in the lower continental crust, also suggesting mafic composition. The North American side of the plate boundary may therefore approach or exceed the seismic velocity of the much-younger mafic oceanic crust in the location of the Craig earthquake (e.g., Rohr et al., 2000).

3. Data and methods

3.1. Aftershock data

A total of 12 GeoPro SediS-V OBS instruments owned and maintained by the University of Texas Institute for Geophysics (UTIG) were deployed for this experiment; eight instruments with usable data were recovered (Fig. 1). The instruments are short-period OBS typically used for offshore active-source experiments; the three-component sensors have a natural frequency of 4.5 Hz and a sample rate of 50 Hz (20 ms). The instruments recorded for 21 days from 28 April 2013 through 19 May 2013, beginning about 4 months after the Craig mainshock. The array covered the southern ~100 km of the ~150 km-long Craig rupture with instruments spaced ~20 km apart (Fig. 1). While the OBS station clocks were dead when they were retrieved, we were able to adjust for clock drift using a linear correction from a previous deployment of the same instruments (Table A1). An individual linear correction for each specific instrument was applied in order to reduce the uncertainty introduced by non-constant drift between clocks (Table A1). Although clock drifts are known to be non-linear (Gardner and Collins, 2012; Gouédard et al., 2014), this timing adjustment seemed sufficient based on a comparison of predicted arrival time versus actual arrival time for a single recorded teleseismic event. The single M_w 6.8 teleseismic event was recorded on 6 OBS stations and occurred on 14 May 2013 at 00:32:25 UTC with an epicenter at 18.728°N, 145.288°E (near the Northern Mariana Islands). Because the instruments were short-period, no other teleseismic arrivals were well-recorded. We further discuss the potential impact of clock drift on our analysis and uncertainty at the end of

section 4.2. OBS data were imported into an Antelope database (www.brtt.com/software) and analyzed using the Antelope software, along with passive data from several nearby land stations from the Alaska Earthquake Center (AEC) and National Earthquake Information Center (NEIC) (Fig. 1).

Using the continuous waveform data from the OBS instruments and land stations, we detected aftershock events using the short-term average/long-term average (STA/LTA) detection algorithm and an automatic event associator and locator. Although our final inversions utilized a total of 1,147 events (of which 1,133 were relocated due to 14 “air” locations), we began by generating a starting catalog of ~100 aftershock events, which were determined using automated detection/location; each of the original events had at least 6 arrivals in the catalog. The initial catalog events were rigorously examined with P and S arrivals re-picked manually using a filter of 3–15 Hz. We then ran a network matched-filter technique (e.g., Walter et al., 2016), which cross-correlates each of the starting catalog events with continuous data to make additional detections. Possible new events with high network correlation coefficients were visually identified and re-picked (yielding a total catalog of 222 events), and the cross-correlation was run again with all 222 events as template events. New detections were again added to the catalog and the network waveform matched-filter was re-run. Using this method and repeating the step with the network waveform matched-filter technique, we were able to detect an order of magnitude more events for a total final, relocated catalog of the aforementioned 1,133 events (e.g., Fig. 1, Fig. 3). We note that our catalog has a similar number of events, despite a significantly shorter time period, than the 2013 Craig aftershock study by Holtkamp and Ruppert (2015), which found 1,785 events during ~5 months following the Craig mainshock using primarily land-based network seismic data. The Holtkamp and Ruppert (2015) catalog is only ~30% complete to magnitude 1.2, while the majority of our events are in the magnitude ~1 range; however, due to poor magnitude calibrations and because magnitudes and moment release are not the focus of this study, we do not further discuss or analyze magnitude data here (see supplementary Fig. A1 and caption for more detail).

While our phase arrivals could have simply been determined from the template event, manual picking after each network waveform matched-filter step was necessary to reduce errors associated with phases for tomography analysis. These phase picks were further improved by computing cross-correlations between cut waveforms of the same components. In this way, cross-correlation travel-time information can be incorporated into the double-difference tomography to improve event locations and the tomography results. Supplement A (Fig. A1) includes a detailed diagram of steps described in this section, including the earthquake catalog generation, network waveform cross-correlation, and phase-arrival time cross-correlation. Phase picks, our starting earthquake catalog, and other data are included as supplementary files with this publication.

Earthquake locations were first determined using a simple grid search algorithm, assuming a 1D velocity model derived from von Huene et al. (1979) appropriate for the Queen Charlotte Terrace (Table A2). This step produced starting hypocenter locations that were then used as input for joint inversion of velocity structure (described in section 3.2) and double-difference location using the conjugate gradient method (LSQR) algorithm. Due to slowness values converging faster than earthquake locations in the joint inversion (Zhang and Thurber, 2003), an iterative double-difference LSQR location-only inversion was run following joint inversion to further improve earthquake locations. In order to best constrain hypocenter depth and location uncertainties, as a separate analysis, we relocated a 21-event subset of events using singular value decomposition (SVD) within the HypoDD software (Waldhauser and

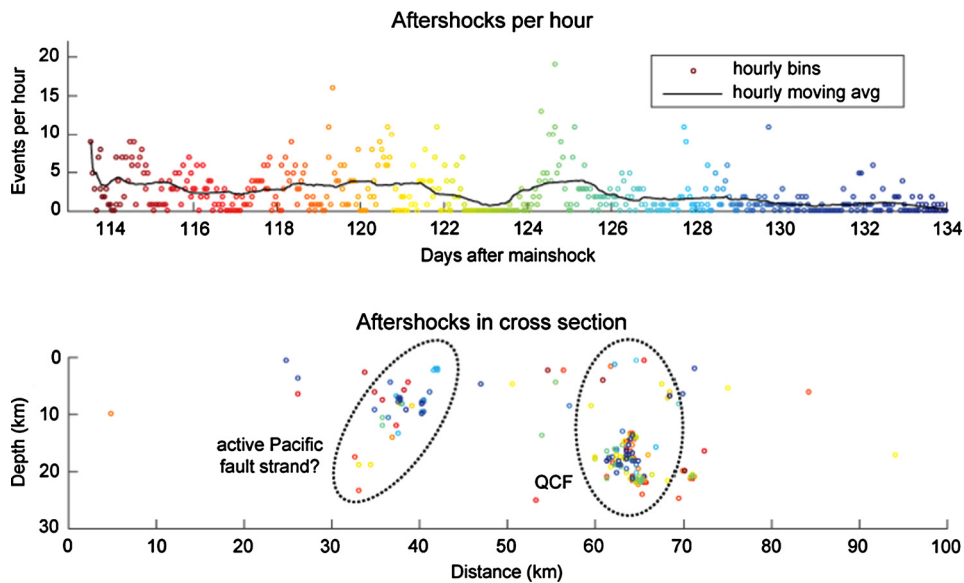


Fig. 3. Spatial distribution of aftershocks used in this study; circles represent events in both plots. Top plot shows the 1,133 relocated events used in this study binned hourly through time, with rainbow colors scaled to indicate time since the 5 January 2013 mainshock. Bottom plot shows a subset of aftershocks located within 15 km of a fault-normal cross-section (cross-section orientation shown in Fig. 1), with color indicating time of the event (as in the top plot). (For interpretation of the colors in the figure(s), the reader is referred to the web version of this article.)

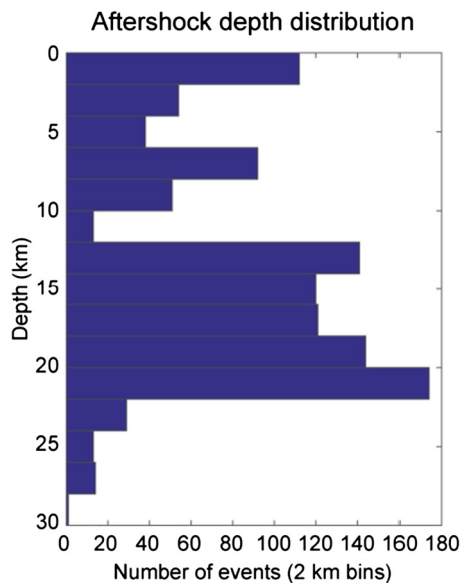


Fig. 4. Histogram showing depth distribution of all 1,133 relocated aftershock events used in this study, with 2 km bins from 0–30 km depths.

Ellsworth, 2000) and the same starting 1D velocity model (von Huene et al., 1979; Table A2). Depths for the 21-event subset of SVD-located events, which are generally some of the largest and best-located events, span ~ 16 – 21 km; these depths are consistent with the dominant depths calculated for smaller events included in our 1,133-event LSQR-located catalog (Fig. 4). SVD-located events within the 16–21 km depth range have calculated uncertainties of ± 1 – 3 km in depth and ~ 1 km in the horizontal directions. These uncertainties should also include any clock drift error. Spatial relocation uncertainty, particularly in depth, should be expected to be higher for events located outside the OBS instrument array, and for smaller events, which may have higher error in traveltime phase picks and/or be observed by fewer stations. All hypocenter relocation data are included with this publication as supplementary files.

3.2. Tomography

To solve for crustal velocities, we use a double-difference arrival-time tomography method (tomoDD) which iteratively attempts to minimize the residual between absolute and predicted arrival times by updating both the relative location between pairs of earthquakes and the 3D velocity model (Zhang and Thurber, 2003). The tomoDD software performs a joint inversion by using double-differencing to relocate event hypocenters, subsequently utilizing the relocated events to solve for 3D velocity structure at user-defined nodes. We weigh catalog and cross-correlation traveltimes following methodology described in recent studies using similar datasets (Froment et al., 2014; McGuire et al., 2015) but use weights tested specifically for our dataset.

TomoDD requires a user-defined starting velocity model, which is then updated during the inversion. Our 1D starting V_p model (Fig. 5, Table A2) was based on Queen Charlotte Terrace velocities from von Huene et al. (1979), which provides a synthesized velocity model from several smaller-scale refraction studies and gravity modeling nearest to our study area. We chose a 1D starting model to avoid introducing an additional variable of poorly constrained lateral heterogeneity, which could possibly influence the results. A constant V_p/V_s ratio of 1.73 was chosen to define S-wave velocities in the initial model. Input velocity models and tomoDD parameters have been provided as supplements with this publication.

A 3D velocity grid used for the inversion process was constructed with a horizontal spacing of 5 km in x and y directions centered directly over the OBS instrument array, with coarser spacing of 10–20 km at the edges of the model outside of the OBS array. The relatively coarse velocity grid was chosen to solve for regional changes in velocity structure, with a focus on the contrast in properties across the fault. We began by inverting for P-wave velocity for catalog events only, introducing cross-correlation events and S-wave arrivals as we reduced traveltime residuals (the time difference between predicted and observed traveltimes). Model node spacing, weighting, smoothing, and other inversion parameters were iteratively tested and re-tested as new data were introduced. Convergence on a relatively smooth velocity model, location errors, and residuals were all considered when

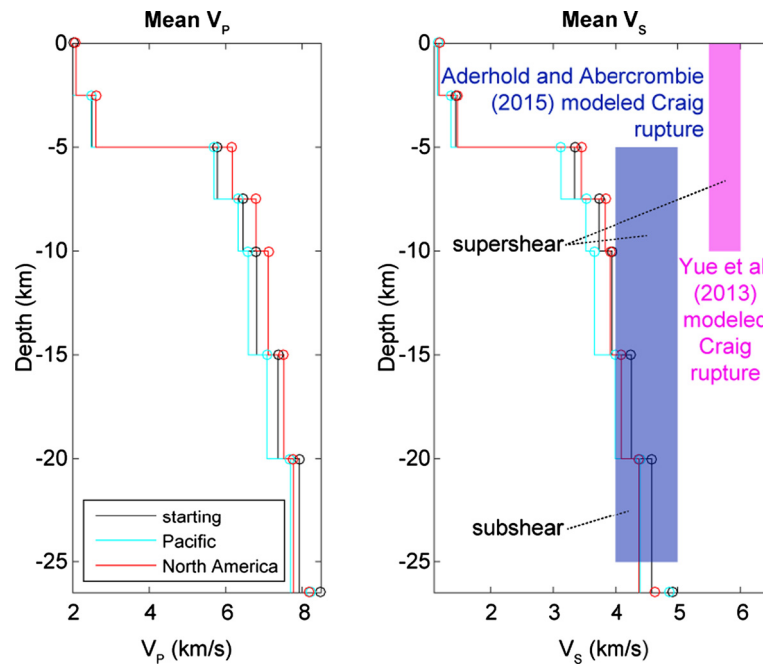


Fig. 5. Depth vs. velocity for modeled V_p and V_s , showing the starting model based on von Huene et al. (1979) and modeled Pacific and North America velocities. Model velocities are defined at the top of each user-defined layer and projected downward through the layer. Mean values plotted here only consider velocities at nodes where Derivative Weight Sum (DWS) > 4 (as shown in Fig. 6). Craig rupture depth ranges from the finite-fault models of Yue et al. (2013) and Aderhold and Abercrombie (2015) are overlain on our V_s model. See Table B1 for actual plotted values. (For interpretation of the colors in the figure(s), the reader is referred to the web version of this article.)

determining final inversion parameters (Table A3). Our final preferred inversion parameters weigh catalog and cross-correlation data equally, and weigh S-wave arrivals more heavily than P-wave arrivals in order to impose a smoother P-wave velocity model (Table A3). Table A4 details the double-difference data used for the inversion. Absolute RMS traveltime residuals were reduced from 1.11 to 0.02 s for cross-correlation events and from 1.25 to 0.28 s for catalog events during the course of the inversion process. Here, we present V_p and V_s slices through the final tomography model at 2.5, 5, 7.5, 10, 15, 20, and 26.5 km depths (Figs. B1–B4). Derivative Weight Sum (DWS) values at each node are a proxy for ray coverage and resolution, and were used to determine the relative sampling of different areas of our model space and identify portions of our model space where we lack resolution (Figs. B5, B6). Here, we only present model results with $DWS > 4$, a somewhat arbitrary threshold selected so as to eliminate obvious outlier data points but still include data interpreted to be reliable (i.e., data consistent with regional trends). Finally, we also calculate V_p/V_s (Fig. B7) and mean velocities (Table B1) for our tomography models. All output velocity data, DWS data, and residuals have been provided as supplements.

3.3. Complementary data

In addition to the OBS aftershock data described above, we utilized several supplementary geophysical datasets to inform our interpretations. GLORIA sidescan sonar data allowed us to interpret the seafloor trace of the QCF (Bruns et al., 1992; Walton et al., 2015). Legacy seismic reflection data were used for both subsurface mapping of QCF-related fault structures (see Walton et al., 2015 for detailed methods and surveys) and for interpretation of structures suggested by the aftershock distribution. One survey of note is USGS survey L378EG, which crosses the fault and OBS array at several locations. We reprocessed line L378EG_954 for this study (Fig. 2; Supplement C), implementing an improved post-stack time migration that provides further detail for structural interpretation.

L378EG processing steps included geometry definition, trace editing, 5–8–60–70 Hz tapered bandpass filter, v^2 gain, multichannel windowed deconvolution, velocity definition, stack, and F–K migration (see Figs. C1 and C2 for uninterpreted before and after images).

4. Observations

4.1. Aftershock distribution

In map view, most seismicity appears to align with the QCF main trace as mapped on the seafloor (Walton et al., 2015), with deeper seismicity lying east of the primary fault strand (Fig. 1). In cross-section, hypocenters indicate a cluster of aftershocks centered around ~ 18 km depth that are likely occurring along the QCF itself (Fig. 3). There is a significant trend of seismicity off of the main trace and on the Pacific Plate side of the boundary (Fig. 1, Fig. 3), which appears to dip steeply away from the main QCF trace. Seismic reflection data indicate the presence of several possible fault strands in the region of the focused Pacific aftershocks (Fig. 2). The 1,133 aftershocks presented in this study occur predominantly at depths from 12–22 km (Fig. 4).

We note that our study time period occurred ~ 4 months after the Craig mainshock and only covers 21 days, limiting our ability to detect and interpret regional and temporal patterns of aftershock occurrence. Holtkamp and Ruppert (2015) notice some temporal variation in a longer ~ 5 month aftershock catalog following the Craig event, namely clusters of events over very short time periods that are aftershocks of larger aftershocks. Despite the short time window of our deployment, our dataset has the distinct advantages of 1) having instruments within close proximity to the source region, and 2) improved azimuthal coverage; namely, instruments located west of the source region. As such, our dataset should provide more reliable spatial information and reduced uncertainties as compared to land-only earthquake catalogs.

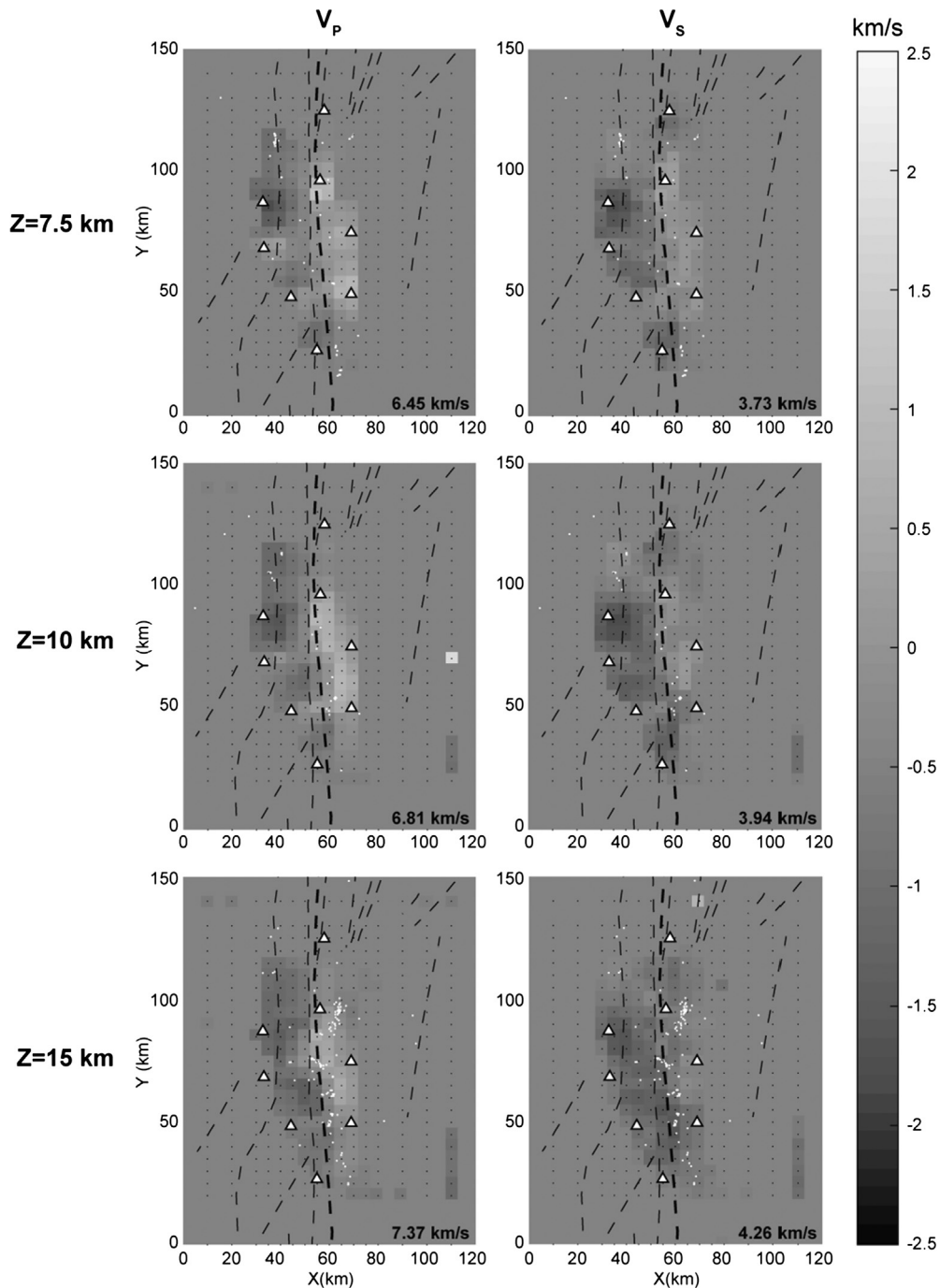


Fig. 6. V_p (left column) and V_s (right column) tomography slices (slice geographic location shown in Fig. 1) showing difference from the starting 1D velocity model value, which is indicated in the bottom right of each panel. Figure highlights 7.5 km (top row), 10 km (middle row), and 15 km (bottom row) depth slices over the survey area. Velocity data corresponding with DWS > 4 are displayed and have not been interpolated, extrapolated, or otherwise filtered in these images. Tomography data are overlain by interpreted sea floor faults (black dashed lines; bold is primary QCF strand) from Walton et al. (2015), aftershock hypocenters (white dots) within 1.25 km (7.5 km slice) and 2.5 km (10 and 15 km slices) of the depth slices, user-defined nodes utilized in velocity inversion (small black dots), and OBS stations (white triangles). Color versions available in Supplement B (Figs. B1, B2).

4.2. Velocity structure

Quantifiable lateral variation in V_p and V_s at depth occurs from 5–20 km (Fig. 5, Fig. 6). Slower V_p and V_s velocities appear dominantly on the Pacific side of the QCF and faster velocities on the North American side through this depth range (Fig. 6). Although the 1D starting model did not include fault geometry, the modeled velocity contrast correlates well with aftershock locations and sea floor fault geometry (Fig. 6). Between depths of 5–20 km, mean V_p and V_s values vary $\sim 6\%$ at most from the starting ve-

locity models (Fig. 5) and total variation across the QCF has a mean of $\sim 3\text{--}11\%$ (Fig. 5, Table B1). When interpreting fault rheology from our models, we note that previous refraction models (e.g., von Huene et al., 1979; Spence and Asudeh, 1993) and seismic reflection interpretation (Rohr et al., 2000) indicate the depth of Mohorovičić discontinuity to be at $\sim 18\text{--}28$ km for the North American Plate (shallowest at the QCF) and $\sim 7\text{--}13$ km for the Pacific Plate near the QCF. Depth to Moho beneath the Pacific crust is likely on the deeper end in our study area due to Pacific Plate downwarping and a significant sediment layer; the top of Pacific

basement has been mapped as deep as 8 s two-way traveltime (TWTT; something like ~ 8 km depth) just south our study area (Walton et al., 2015). In our tomography models at 20 km and deeper, we observe mantle velocities on the Pacific side of the plate boundary and start seeing a slower North American Plate (Fig. 5, Figs. B1–B4). This depth range may be around the lower depth limit of resolution (Figs. B5–B6, Supplement D).

Our results are ultimately limited by the size and quality of our dataset, and we note several limitations and sources of uncertainty. Shallow (< 5 km) and deep (≥ 20 km) tomography results exhibit the least amount of variation from the starting model (Figs. B1–B4). Shallow slices indicate locally fast or slow velocities around OBS instrument locations (generally on the North American and Pacific sides of the QCF, respectively), which lessen or are nonexistent at depths of 7.5 km and deeper (Fig. 6, Figs. B1–B4). These shallow anomalies could be related to a relatively large number of shallow events (Fig. 4) with poorly resolved depths or limited shallow ray coverage indicated by DWS (Supplement B). Below the source region of most of the aftershocks (~ 20 km), model resolution decreases rapidly (Supplement D), leading to little change in velocity structure in tomographic inversion results (Figs. B5, B6). Due to generally lower resolution and/or poor ray coverage in the shallow and deep portions of our model, we only consider depths of 5–20 km in our interpretations. We are able to resolve broad-scale results of our velocity model at 5–20 km depths based on a simplified resolution test (Supplement D, Figs. D1–D8; see also supplementary data files with preferred results); these are also the depths most relevant for understanding the seismogenic zone associated with the 2013 Craig event. Absolute model velocities at these depths are well within reasonable ranges for crystalline oceanic crust, continental crust, and mantle (Fig. 4).

Finally, we acknowledge that our linear clock drift correction may not be optimal; however, based on maximum clock drift calculated from a previous deployment of the same OBS instruments (Table A1), we note that maximum clock drift during our experiment is likely to be considerably less than ~ 50 ms, and that our traveltime residuals can exceed this value, thus encompassing clock-drift errors (Fig. D9). The short duration of our experiment would not allow for significant clock drift to affect the results compared to studies involving months- to year-long OBS deployments. Our residuals are less than the range of worst-case clock drift errors on the order of ~ 100 ms (Gouédard et al., 2014). OBS residuals (Fig. D9) are also Gaussian and zero-mean, suggesting that errors are random and have a similar residual distribution, indicating that clock errors are not biasing the model. OBS residual distributions are similar to residuals on the land instruments, which have GPS-synced clocks, again suggesting that OBS clock errors are not playing a big role in model errors.

5. Discussion

5.1. Implications of event distribution

The Craig centroid was calculated to be at a depth of 13.5 km using a W-phase inversion (Lay et al., 2013) and at a depth of 11–18 km using teleseismic finite fault modeling (Aderhold and Abercrombie, 2015). Our catalog shows aftershocks extending to depths greater than these centroid depths, and deeper than most previously published hypocenter depths for seismicity on the QCF (i.e. USGS; www.usgs.gov). Seismicity deeper than ~ 5 km generally appears to the east of the main fault strand (Fig. 1), supporting a steep eastward dip on the fault; this observation is consistent with the 78° dip on the fault plane found for the Craig event's moment tensor solution (USGS; www.usgs.gov). Aftershocks in our catalog

generally occur at depths of 12–22 km (Fig. 4). The depth distribution suggests stick-slip behavior at depths greater than those observed for most continental strike-slip faults, which tend to have a maximum locking depth of ~ 10 –15 km; for example, a ~ 9 km locking depth has been observed at the onshore Fairweather Fault (Fletcher and Freymueller, 2003). Observed aftershock hypocenters are more consistent with the finite-fault modeling of Aderhold and Abercrombie (2015) in which slip during the Craig event occurred in the zone between 5 and 25 km depths. Our results are less consistent with the rupture model presented by Yue et al. (2013), in which the supershear Craig rupture occurred along a seismogenic zone confined between 0–10 km.

It is possible that the Craig mainshock slipped shallower (< 15 km) areas of the fault interface, consistent with Yue et al. (2013), and that afterslip processes following the Craig event are driving aftershocks at deeper than normal seismogenic depths. Due to our short 21-day deployment ~ 4 months after the mainshock, it is also possible that our dataset is missing trends of shallower seismicity that may have occurred prior to our deployment. However, our catalog provides reliable event locations due to the good azimuthal coverage of our OBS instruments, so our preferred interpretation is that the deeper aftershocks represent deeper stick-slip behavior characteristic of the QCF. The dominance of deeper aftershocks (12–22 km) in our study supports the hypothesis of Rohr et al. (2000) and Aderhold and Abercrombie (2015) that the maximum depth of stick-slip behavior along the QCF is thermally controlled, similar to an oceanic transform fault (e.g., Roland et al., 2010). Our results are therefore more consistent with the expected temperature-dependent rheology of mafic rocks (Boettcher et al., 2007), supporting a fault zone composed of mafic Pacific Plate rocks adjacent to mafic-intermediate North American crustal composition. A deeper, thermally controlled frictional transition out of the seismogenic zone and the occurrence of deeper seismicity along the QCF together might imply that co-seismic slip during the Craig earthquake occurred below 10 km, again consistent with the analysis of Aderhold and Abercrombie (2015).

The aftershock distribution shows evidence for at least one active fault strand within the Pacific crust in the region of the 2013 Craig earthquake (Fig. 1, Fig. 3). Seismic reflection data confirm the presence of offset sedimentary rocks near the seafloor along several faults in this area (Fig. 2). One of these Pacific Plate faults has been interpreted on adjacent seismic reflection profiles along the margin, and seismic reflection data indicate that fault strand could be as long as ~ 200 km (Walton et al., 2015). The minimal vertical sedimentary rock offsets and steep dip of the fault or faults apparent in seismic reflection data (Fig. 2) would suggest a strike-slip or transpressive fault. Holtkamp and Ruppert (2015) identify Craig aftershocks and calculate moment tensor solutions within the Pacific Plate in the region of this same secondary fault. The moment tensor solutions indicate a thrust focal mechanism for at least one of the intra-Pacific Plate events, supporting a transpressional structure here. Other studies (Tréhu et al., 2015; ten Brink et al., 2018) have also interpreted reactivation of Pacific fault strands in order to accommodate regional convergence. The aftershock locations from this study alone are insufficient to infer if or how this or other Pacific fault strands relate structurally to the QCF, and it is also unclear whether this fault played a role in the 2013 Craig mainshock. The clear presence of off-axis aftershock locations, however, provides evidence that various structural features (Fig. 1) may contribute to fault zone heterogeneity and/or strain partitioning in the vicinity of the 2013 Craig rupture. We speculate that these observations of Pacific Plate faulting may also suggest that deformation is preferentially accommodated within the Pacific crust, possibly supporting the hypothesis that the margin consists of a relatively weaker Pacific crust and stronger North American crust along this segment (Tréhu et al., 2015).

5.2. Implications for velocity structure

One of the primary observations of this study is that the Pacific crust is on average ~ 3 – 11% slower in V_P and V_S than the adjacent continental crust at interpreted seismogenic depths well-resolved by our dataset (5–20 km; Table B1), with this contrast particularly sharp across the QCF in the 7.5–15 km depth range (Fig. 6). Consistent with ten Brink et al. (2018), we interpret that the QCF seems to separate the North American crust from the Pacific crust and that we are imaging primarily crustal material in the 7.5–15 km depth range. With a relatively thick (up to ~ 2 km) sedimentary package atop a downwarped Pacific Plate (Walton et al., 2014), these depths likely represent a crust/crust interface across the seismogenic portion of the QCF, or possibly an upper oceanic mantle–continental crust interface at the deeper end of the 7.5–15 km range. We observe mantle velocities on the Pacific side that are similar to North America velocities at 20 km and deeper (Fig. 5, Figs. B1–B4, Table B1). If it were not for the presence of North American accreted terranes, we would expect mafic oceanic rocks, especially deeper gabbroic rocks, to be significantly (up to ~ 1 km/s) faster than granitic continental rocks at an equivalent depth (e.g., Christensen and Mooney, 1995). The crustal architecture of the North American Plate at the location of the Craig event could explain this unexpected velocity contrast across the QCF. The Insular Superterrane makes up the North American crust here and contains higher-velocity mafic rocks (Spence and Asudeh, 1993; Rohr et al., 2000); our study area straddles an area containing primarily Alexander Terrane on the North American side (Colpron and Nelson, 2011; Fig. 1). Although the results of Morozov et al. (1998) describe Insular Superterrane velocities south and inland of our study area, our tomography results are consistent with their findings at shallower crustal depths (5 km; Fig. 5), where our mean continental velocities (6.2 km/s at 5 km) are only slightly above their average values of 5.7–6.0 km/s. Rock type alone could suggest a seismically faster North American crust than was previously presumed in the analysis of possible supershear rupture on this fault (Yue et al., 2013).

Somewhat independent of lithology, the ages of crust on opposing sides of the QCF may also contribute to changes in elastic properties within the crustal rocks of both plates; older, colder crust on the North American side are likely stiffer than the young, warm Pacific crust. The North American crust at the site of the 2013 Craig earthquake is at least Pennsylvanian age (Gardner et al., 1988), and south of the city of Craig, Alaska the Alexander Terrane is as old as Neoproterozoic (Gehrels, 1990). Thus, North American rocks are significantly older than the ~ 15 Ma Pacific Plate oceanic crust here. Relatively low heat flow measurements in the continental crust ~ 350 km south of our study area support an older, colder North American crust (Smith et al., 2003). Considering lithology and age, it is feasible that the North American crust is seismically faster than the Pacific crust in our study area as our results suggest.

There are two alternative explanations for lower Pacific velocities: 1) increased porosity from damage and/or faulting, and 2) mineral alteration (e.g., serpentinization), which generally occurs in higher porosity zones, allowing fluids to influence the chemistry of the upper mantle. Our raypaths may be sampling a broad deformational or damaged zone along the QCF, with deformation preferentially accommodated in a weaker Pacific crust. The QCF cuts through the Queen Charlotte Terrace, which has been deformed by dextral shear and strike-slip faulting during the long history of the QCF (e.g., Rohr et al., 2000). In the region of the 2013 Craig earthquake, the Pacific crust has been deformed and faulted with transpressional splays of the QCF as well as deeper plate-bending faults (Tréhu et al., 2015; Walton et al., 2015). If deformation favors the Pacific crust because it is inherently weaker,

then the deformed terrace and/or Pacific crust could have developed large damaged zones with increased porosity and therefore lower seismic velocity (particularly lower V_S), which could yield velocities significantly slower than the surrounding rock across a broad (~ 5 – 10 km) zone (Roland et al., 2012). S-waves appear to travel predominantly through the North American side of the plate boundary (as indicated by DWS; Figs. B5, B6), potentially supporting higher Pacific deformation, fault-related fracturing, and/or porosity. We also note that V_P/V_S is generally higher on the Pacific side (Fig. B7).

5.3. Implications for supershear rupture

On the basis of regional S-wave observations, the 2013 Craig earthquake was suggested to be a dominantly unilateral rupture, propagating northward at supershear velocities up to 5.5–6.0 km/s (Yue et al., 2013). Theoretical results indicate that supershear ruptures can occur at fault zones where there is a strong material contrast to either side of the fault (e.g., Xia et al., 2005). Based on numerical and physical experiments, the “preferred” slip direction for subshear ruptures (which are generally also sub-Rayleigh, or “normal” earthquakes; e.g., Bouchon et al., 2010) is in the direction of slip of the seismically slower material. Supershear ruptures, however, tend to propagate in the “non-preferred” direction, or the direction of slip of the faster material (Xia et al., 2005). The 2013 Craig earthquake ruptured dominantly northward (Yue et al., 2013) slipping right-laterally between the Pacific crust to the west and North American crust to the east. If our results are correct and the Pacific crust is slower at seismogenic depths relative to the North American crust within the Craig rupture area (Fig. 6), then this relationship would indicate that the 2013 Craig rupture propagated in the opposite direction than that expected for a supershear rupture if the bimaterial interface controls rupture direction.

There are several possible explanations that can reconcile the seemingly incompatible observations of northward Craig supershear rupture and our tomography results. A rupture propagating at 4 km/s within a depth range of 5–25 km, which is the preferred northward rupture model for Aderhold and Abercrombie (2015), would actually be propagating at subshear wave speeds for the seismogenic zone below 15 km based on our tomographic results (Fig. 5, Fig. 6). Thus, one possibility is that the 2013 Craig event may have ruptured at a subshear propagation rate deeper than 15 km, assuming the North American crust is indeed higher velocity at seismogenic depths. We emphasize that the depth range of the Craig event is not well resolved in either the Yue et al. (2013) or Aderhold and Abercrombie (2015) models, and a subshear interpretation relies on coseismic slip deeper than 15 km.

Another possibility is that we are imaging a localized low-velocity, damage, or heterogeneous zone rather than bulk crustal velocities in our tomography model. The limited number of rays from 8 OBS stations may not adequately sample the model domain, such that a thin damage zone may appear wider in the velocity model output. Similarly, small, localized low-velocity anomalies within a heterogeneous regime may appear wider than reality. Understanding the location of the low-velocity zone(s) in relation to the plate boundary is important when considering supershear processes. Numerical models of earthquake ruptures (Harris and Day, 1997) have simulated supershear ruptures under conditions where a fault bisects a low velocity zone. In these models, stress perturbations near the crack tip interfere with waves reflected within the low-velocity zone, generating a complex stress environment for certain dimensions of fault damage zones. Our tomography and fault mapping results, however, are too coarse to determine conclusively whether the QCF bisects any part of the imaged low-velocity zone, a heterogeneous zone, or simply separates low-velocity material from higher-velocity material.

Finally, it is possible that deformation zone width and geometric simplicity play a more significant role in promoting supershear rupture than bulk velocity contrast across the seismogenic zone. For example, the Craig mainshock may have gone supershear due to propagation along a geometrically smooth segment of the QCF (Bouchon et al., 2010; Bruhat et al., 2016). Based on initial results from recent high-resolution geophysical mapping (Brothers et al., 2017), a substantial improvement on the mapping presented here which is based on low-resolution seafloor and legacy seismic reflection data, the main strand of the QCF appears extremely linear with slip highly localized along a single surface trace in the region of the Craig earthquake. Along smoother segments of the QCF, highly localized deformation may potentially produce geometric and stress conditions similar to those observed in other supershear events (Bouchon et al., 2010), allowing the S-wave energy ahead of the crack tip to overcome friction and initiate the secondary, supershear rupture (e.g., Yue et al., 2013).

In any case, our findings suggest that geologic conditions in the region of the Craig earthquake are different from theoretical supershear rupture models requiring a specific contrast in seismic velocity across a bimaterial fault zone. Exceptions to theoretical predictions of rupture propagation direction have been previously noted in the Parkfield region of the San Andreas Fault (Zhao et al., 2010); there, for example, it has been hypothesized that rupture directionality may instead be influenced by structural and stress heterogeneities along the fault. If the 2013 Craig event is also an exception to theoretical propagation of a supershear event along a bimaterial interface, it highlights a need for better understanding of the mechanisms driving supershear rupture and directionality.

6. Conclusions

Our study utilizes a unique OBS earthquake catalog of 1,133 events to examine crustal architecture in the vicinity of the 2013 M_W 7.5 Craig, Alaska earthquake. Using tomographic and seismicity analysis, we find that:

1. The majority of 2013 Craig earthquake aftershocks in our study occur between 12 and 22 km depths (± 3 km), implying that the fault zone is seismogenic at those depths and supporting previous hypotheses that elastic deformation along the QCF is controlled by mafic rheology.
2. Aftershocks within the Pacific Plate highlight possible fault heterogeneity and off-axis seismicity on at least one fault strand within the Pacific crust. The aftershock locations correlate with fault(s) mapped in legacy seismic reflection data.
3. In the vicinity of the 2013 Craig, Alaska earthquake, the Pacific Plate demonstrates P- and S-wave velocities that are ~ 3 –11% slower on average than the North American Plate at seismogenic depths (5–20 km). The contrast in velocity across the fault is especially evident in the 7.5–15 km depth range, coincident with the best-resolved portions of our velocity model and the zone through which the mainshock likely ruptured.
4. The low-velocity zone on the Pacific side of the QCF is consistent with the presence of deformed, faulted rocks within the Pacific Plate and/or Queen Charlotte Terrace, but may also indicate an actual contrast in crustal lithologies across the fault, possibly associated with the Paleozoic–Mesozoic Insular Superterrane accreted to North America.
5. If bimaterial interfaces control supershear rupture directionality, our observation of slower Pacific crust at seismogenic depths is inconsistent with a modeled northward-propagating supershear rupture associated with the Craig event (Yue et al., 2013). This discrepancy may imply a) that the Craig rupture speeds did not exceed the shear-wave speed within the seismogenic zone, b) that the rupture interface is more complex

or deformed than a single fault plane separating relatively intact Pacific and North American crustal material, or c) that there may be controls other than bimaterial contrast, such as fault smoothness, deformation zone width, or the presence of a fault-bisected low-velocity zone, affecting supershear rupture propagation.

Acknowledgments

Support for this project was provided by The University of Texas Jackson School of Geosciences rapid response program, The University of Texas Institute for Geophysics Ewing/Worzel Fellowship, The University of Texas Environmental Science Institute GK-12 Fellowship, the U.S. Geological Survey Alaska Science Center, and the U.S. Geological Survey Pacific Coastal and Marine Science Center. JIW and PJD were supported through USGS Earthquake Hazards Program Grant G15AP00044. Many thanks to the captains and crews of the USCGC *Maple* and *Sycamore* for providing the ship time and personnel assistance for OBS deployment and retrieval. Thanks also to Gail Christeson, Anatoly Mironov, and John Gerbec for their assistance with OBS deployment and retrieval, to Cliff Thurber for supplying the TomoDD code and assisting with its execution, to Uri ten Brink and Nathan Miller for their helpful internal reviews, to Kasey Aderhold and two anonymous reviewers for their peer reviews, and to Danny Brothers and David Walton for additional discussion and assistance. Any use of trade, product, or firm names is for descriptive purposes only and does not imply endorsement by the U.S. Government. This is UTIG contribution #3388.

Appendix A. Supplementary material

Supplementary material related to this article can be found online at <https://doi.org/10.1016/j.epsl.2018.11.021>.

References

- Aderhold, K., Abercrombie, R., 2015. Seismic rupture on an oceanic–continental plate boundary: strike-slip earthquakes along the Queen Charlotte–Fairweather Fault. *Bull. Seismol. Soc. Am.* 105 (2B), 1129–1142.
- Boettcher, M.S., Hirth, G., Evans, B., 2007. Olivine friction at the base of oceanic seismogenic zones. *J. Geophys. Res.* 112 (B1).
- Bostwick, T.K., 1984. A Re-examination of the August 22, 1949 Queen Charlotte Earthquake (M.S. thesis), The University of British Columbia. 126 pp.
- Bouchon, M., Karabulut, H., Bouin, M.-P., Schmittbuhl, J., Vallée, M., Archuleta, R., Das, S., Renard, F., Marsan, D., 2010. Faulting characteristics of supershear earthquakes. *Tectonophysics* 493 (3), 244–253.
- Brothers, D.S., Haeussler, P.J., East, A.E., ten Brink, U., Andrews, B., Dartnell, P., Miller, N.C., Kluesner, J., 2017. A closer look at an undersea source of Alaskan earthquakes. *Eos Trans. AGU* 98.
- Bruhat, L., Fang, Z., Dunham, E.M., 2016. Rupture complexity and the supershear transition on rough faults. *J. Geophys. Res.*
- Bruns, T.R., Stevenson, A.J., Dobson, M.R., 1992. GLORIA Investigation of the Exclusive Economic Zone in the Gulf of Alaska and off Southeast Alaska: M/V Farnella Cruise F7-89-GA, June 14–July 13, 1989. US Department of the Interior, US Geological Survey.
- Christensen, N., Mooney, W., 1995. Seismic velocity structure and composition of the continental crust: a global view. *J. Geophys. Res.* 100, 9761–9788.
- Christeson, G.L., Gulick, S.P.S., van Avendonk, H., Reece, R.S., Worthington, L.L., 2010. The Yakutat Terrane: dramatic change in crustal thickness across the Transition fault, Alaska. *Geology* 38 (10), 895–898.
- Colpron, M., Nelson, J., 2011. A digital atlas of terranes for the northern Cordillera. *BC GeoFile* 2011-11.
- Coney, P.J., Jones, D.L., Monger, J.W., 1980. Cordilleran suspect terranes. *Nature* 288 (5789), 329–333.
- Dehler, S.A., Clowes, R.M., 1988. The Queen Charlotte Islands refraction project. Part I. The Queen Charlotte fault zone. *Can. J. Earth Sci.* 25 (11), 1857–1870.
- DeMets, C., Merkouriev, S., 2016. High-resolution reconstructions of Pacific–North America plate motion: 20 Ma to present. *Geophys. J. Int.* 207 (2), 741–773.
- Doser, D.I., Rodriguez, H., 2011. A seismotectonic study of the southeastern Alaska region. *Tectonophysics* 497 (1), 105–113.
- Doubrovine, P.V., Tarduno, J.A., 2008. A revised kinematic model for the relative motion between Pacific oceanic plates and North America since the Late Cretaceous. *J. Geophys. Res.* 113 (B12).

- Dunham, E.M., Archuleta, R.J., 2004. Evidence for a supershear transient during the 2002 Denali fault earthquake. *Bull. Seismol. Soc. Am.* 94 (6B), S256–S268.
- Elliott, J.L., Larsen, C.F., Freymueller, J.T., Motyka, R.J., 2010. Tectonic block motion and glacial isostatic adjustment in southeast Alaska and adjacent Canada constrained by GPS measurements. *J. Geophys. Res.* 115 (B9), B09407.
- Fletcher, H.J., Freymueller, J.T., 2003. New constraints on the motion of the Fairweather fault, Alaska, from GPS observations. *Geophys. Res. Lett.* 30 (3), 1139.
- Froment, B., McGuire, J.J., Hilst, R., Gouédard, P., Roland, E.C., Zhang, H., Collins, J.A., 2014. Imaging along-strike variations in mechanical properties of the Gofar transform fault, East Pacific Rise. *J. Geophys. Res.* 119 (9), 7175–7194.
- Gardner, A.T., Collins, J.A., 2012. Advancements in high-performance timing for long term underwater experiments: a comparison of chip scale atomic clocks to traditional microprocessor-compensated crystal oscillators. Paper presented at Oceans, 2012, IEEE.
- Gardner, M., Bergman, S., Cushing, G., MacKevett, E., Plafker, G., Campbell, R., Dodds, C., McClelland, W., Mueller, P., 1988. Pennsylvanian pluton stitching of Wrangellia and the Alexander terrane, Wrangell Mountains, Alaska. *Geology* 16 (11), 967–971.
- Gehrels, G.E., 1990. Late Proterozoic–Cambrian metamorphic basement of the Alexander terrane on Long and Dall Islands, southeast Alaska. *Bull. Geol. Soc. Am.* 102 (6), 760–767.
- Gouédard, P., Seher, T., McGuire, J.J., Collins, J.A., van der Hilst, R.D., 2014. Correction of ocean-bottom seismometer instrumental clock errors using ambient seismic noise. *Bull. Seismol. Soc. Am.* 104 (3), 1276–1288.
- Gulick, S., Reece, R., Christeson, G., van Avendonk, H., Worthington, L., Pavlis, T., 2013. Seismic images of the Transition fault and the unstable Yakutat–Pacific–North American triple junction. *Geology* 41 (5), 571–574.
- Haeussler, P.J., Bradley, D.C., Wells, R.E., Miller, M.L., 2003. Life and death of the Resurrection plate: evidence for its existence and subduction in the northeastern Pacific in Paleocene–Eocene time. *Bull. Geol. Soc. Am.* 115 (7), 867–880.
- Harris, R.A., Day, S.M., 1997. Effects of a low-velocity zone on a dynamic rupture. *Bull. Seismol. Soc. Am.* 87 (5), 1267–1280.
- Holtkamp, S., Ruppert, N., 2015. A high resolution aftershock catalog of the magnitude 7.5 Craig, Alaska, earthquake on 5 January 2013. *Bull. Seismol. Soc. Am.* 105 (2B), 1143–1152.
- Horn, J., Clowes, R., Ellis, R., Bird, D., 1984. The seismic structure across an active oceanic/continental transform fault zone. *J. Geophys. Res.* 89 (B5), 3107–3120.
- Hyndman, R., Hamilton, T., 1993. Queen Charlotte area Cenozoic tectonics and volcanism and their association with relative plate motions along the northeastern Pacific margin. *J. Geophys. Res.* 98 (B8), 14257–14277.
- Lay, T., Ye, L., Kanamori, H., Yamazaki, Y., Cheung, K.F., Kwong, K., Koper, K.D., 2013. The October 28, 2012 Mw 7.8 Haida Gwaii underthrusting earthquake and tsunami: slip partitioning along the Queen Charlotte Fault transpressional plate boundary. *Earth Planet. Sci. Lett.* 375, 57–70.
- Mackie, D., Clowes, R., Dehler, S., Ellis, R., Morel-À-l'Huissier, P., 1989. The Queen Charlotte Islands refraction project. Part II. Structural model for transition from Pacific plate to North American plate. *Can. J. Earth Sci.* 26 (9), 1713–1725.
- McGuire, J.J., Lohman, R.B., Catchings, R.D., Rymer, M.J., Goldman, M.R., 2015. Relationships among seismic velocity, metamorphism, and seismic and aseismic fault slip in the Salton Sea Geothermal Field region. *J. Geophys. Res.* 120 (4), 2600–2615.
- Morozov, I.B., Smithson, S.B., Hollister, L.S., Diebold, J.B., 1998. Wide-angle seismic imaging across accreted terranes, southeastern Alaska and western British Columbia. *Tectonophysics* 299 (4), 281–296.
- Plafker, G., Nokleberg, W., Lull, J., 1989. Bedrock geology and tectonic evolution of the Wrangellia, Peninsular, and Chugach Terranes along the Trans-Alaska Crustal Transect in the Chugach Mountains and Southern Copper River Basin, Alaska. *J. Geophys. Res.* 94 (B4), 4255–4295.
- Rohr, K.M.M., 2015. Plate boundary adjustment of the southernmost Queen Charlotte fault. *Bull. Seismol. Soc. Am.* 105 (2b), 1076–1089.
- Rohr, K.M.M., Scheidhauer, M., Trehu, A.M., 2000. Transpression between two warm mafic plates—the Queen Charlotte Fault revisited. *J. Geophys. Res.* 105 (B4), 8147–8172.
- Roland, E., Behn, M.D., Hirth, G., 2010. Thermal–mechanical behavior of oceanic transform faults: implications for the spatial distribution of seismicity. *Geochem. Geophys. Geosyst.* 11 (7).
- Roland, E., Lizarralde, D., McGuire, J.J., Collins, J.A., 2012. Seismic velocity constraints on the material properties that control earthquake behavior at the Quebrada-Discovery-Gofar transform faults, East Pacific Rise. *J. Geophys. Res.* 117 (B11).
- Schell, M.M., Ruff, L.J., 1989. Rupture of a seismic gap in southeastern Alaska: the 1972 Sitka earthquake (Ms 7.6). *Phys. Earth Planet. Inter.* 54 (3), 241–257.
- Shi, Z., Ben-Zion, Y., 2006. Dynamic rupture on a bimaterial interface governed by slip-weakening friction. *Geophys. J. Int.* 165 (2), 469–484.
- Smith, A., Hyndman, R., Cassidy, J., Wang, K., 2003. Structure, seismicity, and thermal regime of the Queen Charlotte Transform Margin. *J. Geophys. Res.* 108 (B11).
- Smith, W.H.F., Sandwell, D.T., 1997. Global sea floor topography from satellite altimetry and ship depth soundings. *Science* 277 (5334), 1956–1962.
- Spence, G.D., Asudeh, I., 1993. Seismic velocity structure of the Queen Charlotte Basin beneath Hecate Strait. *Can. J. Earth Sci.* 30 (4), 787–805.
- ten Brink, U., Miller, N., Andrews, B., Brothers, D., Haeussler, P., 2018. Deformation of the Pacific/North America plate boundary at Queen Charlotte Fault: the possible role of rheology. *J. Geophys. Res.*
- Tréhu, A.M., Scheidhauer, M., Rohr, K.M.M., Tikoff, B., Walton, M.A.L., Gulick, S.P.S., Roland, E., 2015. An abrupt transition in the mechanical response of the upper crust to transpression across the Queen Charlotte Fault. *Bull. Seismol. Soc. Am.* 105 (2B), 1114–1128.
- von Huene, R., Shor Jr, G.G., Wageman, J., 1979. Continental margins of the eastern Gulf of Alaska and boundaries of tectonic plates. In: *Geological and Geophysical Investigations of Continental Margins*. In: American Association of Petroleum Geologists Memoir, vol. 29, pp. 273–290.
- Waldhauser, F., Ellsworth, W.L., 2000. A double-difference earthquake location algorithm: method and application to the northern Hayward fault, California. *Bull. Seismol. Soc. Am.* 90 (6), 1353–1368.
- Walter, J.I., Dotray, P.J., Frohlich, C., Gale, J.F., 2016. Earthquakes in northwest Louisiana and the Texas–Louisiana border possibly induced by energy resource activities within the Haynesville Shale Play. *Seismol. Res. Lett.* 87 (2A).
- Walton, M.A.L., Gulick, S.P.S., Haeussler, P.J., Roland, E., Tréhu, A.M., 2015. Basement and regional structure along strike of the Queen Charlotte Fault in the context of modern and historical earthquake ruptures. *Bull. Seismol. Soc. Am.* 105 (2B), 1090–1105.
- Walton, M.A.L., Gulick, S.P.S., Reece, R.S., Barth, G.A., Christeson, G.L., Van Avendonk, H.J.A., 2014. Dynamic response to strike-slip tectonic control on the deposition and evolution of the Baranof Fan, Gulf of Alaska. *Geosphere* 10 (4), 680–691.
- Xia, K., Rosakis, A.J., Kanamori, H., Rice, J.R., 2005. Laboratory earthquakes along inhomogeneous faults: directionality and supershear. *Science* 308 (5722), 681–684.
- Yue, H., Lay, T., Freymueller, J.T., Ding, K., Rivera, L., Ruppert, N.A., Koper, K.D., 2013. Supershear rupture of the 5 January 2013 Craig, Alaska (Mw 7.5) earthquake. *J. Geophys. Res.* 118 (11), 5903–5919.
- Zhang, H., Thurber, C., 2003. User's Manual for TomoDD1.1 (Double-Difference Tomography) for Determining Event Locations and Velocity Structure from Local Earthquakes and Explosions. Department of Geology and Geophysics, University of Wisconsin–Madison, Madison, WI.
- Zhao, P., Peng, Z., Shi, Z., Lewis, M.A., Ben-Zion, Y., 2010. Variations of the velocity contrast and rupture properties of M6 earthquakes along the Parkfield section of the San Andreas fault. *Geophys. J. Int.* 180 (2), 765–780.